An IMU-Based Ground Reaction Force Estimation Method and Its Application in Walking Balance Assessment

Xiangzhi Liu, Xiangliang Zhang, Bin Zhang, *Senior Member, IEEE*, Bin Zhou, Zexia He, and Tao Liu, *Senior Member, IEEE*

***Abstract*— Walking is one of the most common daily movements of the human body. Therefore, quantitative evaluation of human walking has been commonly used to assist doctors in grasping the disease degree and rehabilitation process of patients in the clinic. Compared with the kinematic characteristics, the ground reaction force (GRF) during walking can directly reflect the dynamic characteristics of human walking. It can further help doctors understand the degree of muscle recovery and joint coordination of patients. This paper proposes a GRF estimation method based on the elastic elements and Newton-Euler equation hybrid driving GRF estimation method. Compared with the existing research, the innovations are as follows. 1) The hardware system consists of only two inertial measurement units (IMUs) placed on shanks. The acquisition of the overall motion characteristics of human walking is realized through the simplified four-link walking model and the thigh prediction method. 2) The method was validated not only on 10 healthy subjects but also on 11 Parkinson's patients and 10 stroke patients with normalized mean absolute errors (NMAEs) of 5.95%±1.32%, 6.09%±2.00%, 5.87%±1.59%. 3) This paper proposes a dynamic balance assessment method based on the acquired motion data and the estimated GRF. It evaluates the overall balance ability and fall risk at four key time points for all subjects recruited. Because of the low-cost system, ease of use, low motion interference and environmental constraints, and high estimation accuracy, the proposed GRF estimation method and walking balance automatic assessment have broad clinical value.**

***Index Terms*— Wearable sensor system, gait analysis, ground reaction force (GRF) estimation, walking balance assessment, clinical application.**

I. Introduction

NEUROLOGICAL diseases can disrupt the human's normal motion control, leading to decreased balance ability and increased risk of falls [1]. Therefore, the quantitative evaluation of the balance ability is significant for doctors to grasp the disease severity and the effect of rehabilitation in the clinic. There are many ways to evaluate the balance of the human clinically [2], [3], [4], [5]. However, the clinical evaluation of walking balance is still at the scale stageThe subjective scoring of the patient's walking balance ability is based on the doctor's observation and professional experience. This subjective evaluation will inevitably lead to different evaluation results. For example, the evaluation result for the same generalized Parkinson's patient from two physicians using the Unified Parkinson's Disease Rating Scale (UPDRS) gait task can have a 25% difference [6].

With the development of micro-electromechanical systems (MEMS) technology, wearable technology is suitable for the requirements of portability and low interference of instruments in clinic. Therefore, many studies [7], [8], [9], [10] were reported to quantify the walking state through wearable sensors to evaluate the motion control ability of the subjects. Advancements were also made in quantifying walking balance through wearable devices [11], [12], [13], [14]. These researches showed that the wearable sensor can quickly and objectively estimate Patient's level of impairment. Moreover, in order to obtain more comprehensive quantitative results of walking balance, researchers often are required to obtain the GRF to quantify balance ability of the human body [15], [16], [17]. Current measurements of GRF often rely on rigid force sensing shoes, force-measuring insoles, or force-measuring plates [18], [19], [20].

Manuscript received 31 August 2023; revised 19 November 2023 and 13 December 2023; accepted 19 December 2023. Date of publication 28 December 2023; date of current version 16 January 2024. This work was supported in part by NSFC under Grant 52175033 and Grant U21A20120; in part by the Key Research and Development Program of Zhejiang under Award 2023C03196, Award 2022C03103, and Award 2021C03051; and in part by the Zhejiang Provincial Natural Science Foundation of China under Grant LZ20E050002. *(Corresponding author: Tao Liu.)*

This work involved human subjects or animals in its research. Approval of all ethical and experimental procedures and protocols was granted by the Medical Ethics Committee of the School of Biomedical Engineering and Instrument Science, Zhejiang University under Application No. 2021-39.

Xiangzhi Liu, Xiangliang Zhang, Zexia He, and Tao Liu are with the State Key Laboratory of Fluid Power and Mechatronic Systems, School of Mechanical Engineering, Zhejiang University, Hangzhou 310027, China (e-mail: liuxiangzhi@zju.edu.cn; xlzh@zju.edu.cn; zexia_he@zju.edu.cn; liutao@zju.edu.cn).

Bin Zhang is with the Department of Electrical Engineering, University of South Carolina, Columbia, SC 29208 USA (e-mail: zhangbin@cec.sc.edu).

Bin Zhou is with the Hangzhou Pudixin Rehabilitation Hospital, Hangzhou 311200, China (e-mail: 632032346@qq.com).

Digital Object Identifier 10.1109/TNSRE.2023.3347729

TABLE I
GRF INDIRECT MEASUREMENTS RESULT FROM RELATED WORK

Researcher	Error(Type)	Hardware	Experimenters	Methods
Shahabpoor [23]	7%(PNME)	3 IMUs	6 Health	Rm
Karatsidis [24]	5.3%(FNME)	17 IMUs	11 Health	NEe&Rm
Tan [25]	5.4%(FNME)	8 IMUs	12 Health	MLa
Refai [26]	12.1±3.3%(FNME)	1 IMU	8 Health	EEKF
Hossain [27]	5.49±4.36%(FNME)	3 IMUs for	Dataset A-20 Health	MLa
	7.86±1.10%(FNME)	single limb	Dataset B-17 Health	MLa
Bach [28]	8.6±2.3%(FNME)	2 IMUs	21 Health	MLa
Ripic [31]	3.2±5.7%(FNME)	Kinect	10 Health	Mm
Eltoukhy [32]	2%-15%(FNME)	Kinect	9 PD	Mm

*PD denotes Parkinson's disease, Rm denotes Regression model, NEe denotes Newton–Euler equations, MLa denotes Machine Learning algorithm, EEKFs denotes Extended Kalman filter, Mm denotes Musculoskeletal model, PNRMSE denotes peak-to-peak normalized mean error, FNME denotes Full period normalized mean error.

However, these instruments' drawbacks, including the cost, weight, and environmental limitations, have greatly weakened the advantages they offer [21], [22]. As shown in TABLE I, many scholars [23], [24], [25], [26], [27], [28] have also studied the indirect ways to obtain GRF through lighter and low-cost wearable sensors (such as IMU) to satisfy the acquisition of force and reduce motion interference. Shahabpoor et al. [23] proposed a linear model with low computing requirements and successfully estimated GRF through three IMUs placed on C7, L5, and one of the thighs of the human body. The method was validated on 6 healthy subjects, and the peak to peak error of vertical GRF was controlled at 7%. Hossain et al. [27] placed three IMUs on the thigh, shank, and foot of the subject's unilateral limb and completed GRF estimation through the proposed Kinetics-FM-DLR-Ensemble-Net. The proposed method was verified on two public datasets [29], [30], demonstrating the feasibility of deep learning in plantar force estimation. Refai et al. [26] placed an IMU on the pelvis to collect the center-of-mass acceleration during walking and established the mapping relationship between the center-of-mass acceleration and GRF through the extended Kalman filter. They compared the prediction results of 8 healthy subjects with the GRF results collected directly by the ForceShoe system. The error is 12.1 $\pm$ 3.3%.

Despite these successes, some issues still need to be solved in current research on motion sensor-based GRF prediction. One is that the proposed methods are often too complex to meet the needs of real-time computing in the clinic. The second is that they often require too many motion sensors, which weakens wearable sensors' advantages. Third, the current mainstream GRF prediction research is still oriented to healthy people, and the clinical application effect needs to be further verified.

This work proposes a method to estimate GRF using only two IMUs placed on the shank to address the above-mentioned limitations. The novelty of the proposed method is that it adds some virtual elastic force units on the shanks and thighs to adapt to differences in gait performance between patients with different neurological disorders and health. Experimental results and comparison studies on 21 patients and 10 healthy subjects demonstrate the efficiency of the proposed method. More importantly, this work also proposes an evaluation of walking balance, quantifying the risk of falls in patients and healthy subjects.

TABLE II
EXPERIMENTERS INFORMATION SHEET

Subject	Size	Height/m	Weight/Kg	Age/year
Health	10	1.72±0.12	67±5	26±4
Stroke patients	10	1.64±0.08	65±10	66±14
Parkinson's patients	11	1.67±0.09	64±12	68±12

II. MATERIAL AND METHOD

A. Participants and Protocols

This study was approved by the Medical Ethics Committee of the School of Biomedical Engineering and Instrument Science, Zhejiang University(Project identification code: 2021-39). This research recruited 10 healthy subjects, 10 Stroke patients, and 11 Parkinson's patients (shown in TABLE II) for the experiments. All the recruited patients can walk independently without external assistance for experimental safety and to exclude interference with force measurements by external auxiliary devices. Each subject was asked to walk 10 meters in a straight line (in the clinical rehabilitation gym) 3 times. They keep still for 5 seconds before and after walking each time as static correction data, which is used to correct the error caused by IMUs' wearing offset.

As shown in Fig. 1-(1), the experimental data acquisition system consists of kinematics acquisition equipment and force acquisition equipment. The kinematics collection device is Fuzhi^{TM}-gait (Zhejiang FuZhi Technology & Innovation Co., Ltd., Hangzhou, China), which collects three-axis acceleration, three-axis angular velocity, and three-axis magnetometer data in real-time. The maximum acquisition frequency of the IMU is 100Hz. To minimize the impact of the external magnetic field on the IMU data acquisition, the experiments are conducted in the clinical rehabilitation gym, which is an open area without any other electrical equipment. Considering that the recruited patients have unstable gait performance and need to stay in the hospital for a long time, wearable devices that can measure continuous gait cycles are used instead of force plates that can only collect a single gait cycle per experiment.

The GRF collection device mainly uses force-sensing shoes consisting of two commercial SRI force sensors (M3705C, Sunrise Instruments, Inc., Shanghai, China) for each shoe. The same shoes were also used in other researches [33], [34], [35]. The force-sensing shoe consists of two force sensors placed on the toe and sole, respectively, which can collect three-dimensional force and three-dimensional moments in real-time. To further verify the reliability of the wearable measurement of GRF, the GRF measured by force-sensing shoes is then compared with two six-dimensional force plates (AMTI, US), which are recognized as the gold standard for GRF measurement.

B. Force Estimation for Single Support Phase

Based on the existing research [24], the GRF during the single support phase of gait can be solved by the Newton-Euler equation. To improve the algorithm solution speed and reduce the number of sensor nodes, a simplified human walking model is proposed, which includes a four-link model composed of hip

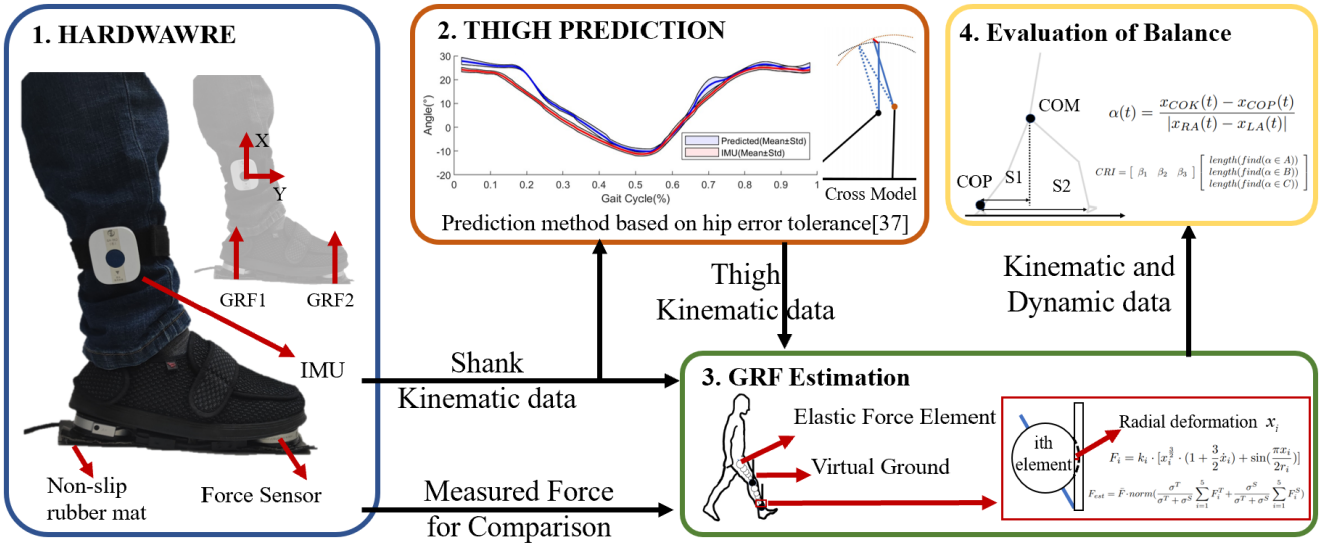

Fig. 1. Overall algorithm block diagram.

TABLE III
SEGMENTS DEFINITION IN OUR PAPER

Subject	m(%)	COM(%)	Proximal	Distal
Upper body	60.28	100.00	Hip	Hip
Left thigh	14.16	40.95	Hip	Knee
Right thigh	14.16	40.95	Hip	Knee
Left shank	5.70	57.26	Knee	Ankle
Right shank	5.70	57.26	Knee	Ankle

*The simplified walking model is only a four-link model composed of two thighs and shanks, so the weight and COM of the upper body are concentrated on the hip joint. In addition, the foot is also simplified in this model, and the mass is concentrated on the ankle joint, so the mass ratio and mass center position of the shanks are different from those of the original model.

joints, left and right knee joints, and left and right ankle joints. As shown in the TABLE III, based on the existing human segment data [36] and the simplified walking model, the mass and center of mass (COM) of all the segments in the simplified walking model could be obtained.

As shown in Fig. 1-(2), based on our previous research results on gait [37], two IMUs were placed on the shanks to estimate the position of the thigh and have been verified on healthy subjects and patients. Similarly, the gait events have been identified through the IMUs' motion data placed on the shanks, and the velocity and displacement trajectory in continuous gait cycles can be calculated. By Eqs.(1), the velocity of the knee joint could be obtained.

$$\begin{cases} \vec{v}_{knee} = \vec{v}_{IMU} + \vec{\omega}_{IMU} \times \vec{L}_{IMU} \\ \vec{x}_{knee} = \vec{x}_{IMU} + \vec{L}_{IMU} \end{cases} \tag{1}$$

where $\vec{v}_{knee}$ and $\vec{v}_{IMU}$ are the velocity vectors of the knee joint and IMU attached on the shank, respectively, $\vec{\omega}_{IMU}$ is the angular velocity of the shank, which is directly obtained by the IMU, $\vec{L}_{IMU}$ is the length vector from the place where the IMU is attached to the knee joint. Similarly, $\vec{x}_i$ represents the position vector of the joints.

In summary, the real-time poses of the shank and thigh in the simplified walking model can be obtained. Moreover, the motion trajectory of the hip joint can be obtained through Eqs.(2), which is used to represent the position change of the upper body.

$$\begin{cases} \vec{v}_{upper\_body} = \vec{v}_{hip} = \vec{v}_{knee} + \vec{\omega}_{thigh} \times \vec{L}_{thigh} \\ \vec{x}_{upper\_body} = \vec{x}_{hip} = \vec{x}_{knee} + \vec{L}_{thigh} \end{cases} \tag{2}$$

where $\vec{v}_{upper\_body}$ and $\vec{v}_{hip}$ are the velocity vectors of the upper body and hip joint, respectively, $\vec{\omega}_{thigh}$ is the angular velocity of the thigh, which can be obtained by deriving the estimated thigh position, $\vec{L}_{thigh}$ is the length vector from the knee joint to the hip joint. Similarly, $\vec{x}_i$ represents the position vector of the joints. Note that they are equivalent when the model assumes the mass of the upper body is concentrated in the hip.

Since the kinematic data of all joints in the simplified model could be obtained by Eqs.(2), the GRF for the single support phase during walking could be calculated through Eqs.(3).

$$\vec{F}_{ground} = \sum_{1}^{5} [m_i \cdot (\vec{a}_i - g)] \tag{3}$$

where $\vec{F}_{ground}$ is the estimated GRF vector, including vertical support force and horizontal friction force, m_i and $\vec{a}_i$ are the mass and mass center's acceleration vectors of each segment of the model, respectively.

Since the force only acts on one foot in the single support phase of walking, the external force of the model is precisely the GRF.

C. Force Estimation for Double Support Phase

Unlike the single support phase, the external force is shared by two feet in the double support phase, and the sharing ratio is uncertain. Therefore, a new model is needed to determine the GRF of different feet.

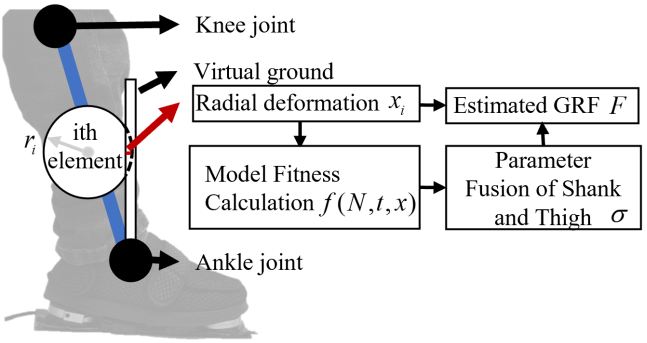

Fig. 2. Force calculation flow chart for double support phase.

Previous studies [38], [39] revealed a strong correlation between foot movement and GRF, which can be used to estimate GRF changes indirectly. Some studies [23], [40] also showed that the correlation between lower limb motion data and GRF is higher than that between foot motion data. Therefore, as shown in Fig. 1-(3), some elastic force units were placed on the shanks and thighs for higher accuracy.

1) Elastic Elements Settings: A total of 5 adjacent elastic elements are placed on the shanks and thighs, respectively, to simulate the change of GRF during walking. The centers' positions of the five elastic elements are evenly distributed in the five equal parts of the limbs. Elastic unit settings can be found in Hertz/Hunt and Crossley model [41], also used in Simbody. The radio of the second to the fifth elastic elements can be calculated as:

$$\begin{cases} r_i^S = \phi(i) * r_1^S \\ r_i^T = \psi(i) * r_1^T \end{cases} \tag{4}$$

where r_i^s and r_i^t are the radius of the i-th elastic element of the shanks and thighs, respectively, $\phi(i)$ and $\psi(i)$ are the length increment coefficients of the shanks and thighs, respectively, which can be obtained by Eqs.(5) and is used to ensure that the GRF output by the model is smooth enough.

$$\begin{cases} \phi(i) = \frac{1}{3}(2 + \frac{i+1}{1+e^{-2(i-1)}}) \\ \psi(i) = \sqrt{i} \end{cases} \tag{5}$$

The definition of elastic element law can calculate the radius of the first elastic element that the elastic body radius is the distance between the center of the element and the virtual ground when deformation is about to occur. When the gait is in the heel strike event, the foot interacts with the ground, resulting in GRF. More specifically, the elastic deformation of the first elastic element has just occurred at this time. The distance between the center of the first elastic element and the virtual ground can be calculated as:

$$r_1^T = \frac{1}{5} \cdot L_{thigh} \cdot \sin(\theta^T(HS)) \tag{6}$$

where r_1^T is the radius of the first elastic element placed on the thigh in the current gait cycle, $\theta^T(HS)$ is the attitude angle of the thigh when the heel strikes ground in the current gait cycle. Similarly, the radius of the first elastic element placed on the shanks can be calculated.

2) Parameter Fusion Calculation: Using the above method, we set the center position and radius of all the elastic elements attached to the shanks and thighs. The deformation of the elastic elements can be obtained through the attitude angle data of the shanks and thighs in the current gait cycle to calculate two kinds of simulated forces (from the thighs and shanks, respectively).

$$x_i^T(t) = r_i^t - \frac{i}{5} \cdot L_{thigh} \cdot \sin(\theta^T(t)) \tag{7}$$

where $x_i^T(t)$ is the deformation of the i-th elastic thigh element at time t.

The weighting of the two simulated forces to the final estimated GRF is uncertain. Due to the differences in exercise habits, health status, height, and weight of each subject, using a fixed ratio to weight the average will significantly reduce the adaptability of the model. Considering that the weight coefficient means the correlation between the different limb motion data and the final GRF, we propose a model fitness calculation method that includes the number of elastic element activation, the activation time of elastic units, and the degree of activation. First, we need to calculate the elastic units' time and deformation characteristics. Taking the thigh as an example, The time characteristic $\tilde{t}_{start}^T$, given by the Eqs.(8), comprises the gait phases in which different elastic bodies begin to deform, reflecting the rate at which the model affects human walking.

$$\tilde{t}_{start}^T = [\, t_{start\_1}^T \ \cdots \ t_{start\_5}^T \,] \tag{8}$$

where $\tilde{t}_{start}^{T\_i}$ is the activation start time of the i-th elastic elements of the thigh, which is normalized by the current gait cycle, and the value is between 0 and 1.

Similarly, the elastic units' deformation characteristic $\tilde{x}_{end}^T$, given by the Eqs.(9), is the elastic units' deformation when the contra-lateral toe is off the ground (at the end of the double support period). That reflects the role of the model in the entire gait process.

$$\tilde{x}_{end}^T = [\, x_1^T(TO) \ \cdots \ x_5^T(TO) \,] \tag{9}$$

where TO is the time when the contra-lateral toe is off the ground.

Based on the obtained time characteristics $\tilde{t}_{start}^T$ and deformation characteristics $\tilde{x}_{end}^T$, model fitness given by the Eqs.(10) can be used to determine the impact weight of the two simulated forces on the final estimated GRF.

$$\sigma^T = f(N, \tilde{t}_{start}^T, \tilde{x}_{end}^T) = N \cdot \sum_{i=1}^{5} [\frac{\tilde{x}_{end}^T(i)}{(\tilde{t}_{start}^T(i)+1)^3 \cdot e^{\tilde{t}_{start}^T(i)}}] \tag{10}$$

where σ^T is the model fitness of the thigh, and the shank's fitness can also be calculated by the same method, $f()$ is the fitness calculation function, N is the number of elastic element activation.

3) GRF Estimation for Double Support Phase: After defining all elastic body properties and computing deformations, the estimated GRF can be calculated from the Hertz/Hunt and Crossley model. By combining our needs, the constant terms of the original contact force model can be normalized, and the final calculation method for a single elastic body is as follows:

$$F_i = k_i \cdot [x_i^{\frac{3}{2}} \cdot (1 + \frac{3}{2}\dot{x}_i) + \sin(\frac{\pi x_i}{2r_i})] \tag{11}$$

where F_i is the normalized force of i-th elastic element, k_i is the elastic coefficient of the i-th elastic unit, and the value of which is equal to $1 + 0.1i$, sin() is to increase the nonlinear proportion of the deformation force of the elastic element, making the GRF transition smoother.

After calculating the deformation force of all elastic elements of the shanks and thighs and the model fitness of the limbs, the estimated GRF can be finally calculated as:

$$F_{est} = \bar{F} \cdot norm(\frac{\sigma^T}{\sigma^T + \sigma^S} \sum_{i=1}^{5} F_i^T + \frac{\sigma^S}{\sigma^T + \sigma^S} \sum_{i=1}^{5} F_i^S) \tag{12}$$

where F_{est} is the estimated GRF, $\bar{F}$ is the mean of $\vec{F}_{ground}$, $norm()$ is the normalized function used to scale the results in the current gait cycle to 0 to 1, σ^S and F_i^S are the model fitness and elastic element force of the shanks, respectively.

In summary, we have successfully transformed from human kinematics measurement to dynamics estimation through methods such as elastic element characteristic design, limb model fitness calculation, and GRF weighted calculation.

D. Evaluation of Walking Balance

Evaluating the human's walking balance ability is significant for predicting falls. Based on obtaining the kinematics and dynamics data of the simplified model of the human body, a quantitative evaluation of the walking balance ability of the human body can be conducted.

Walking balance can be assessed by the quantity of the displacement of the center of kinematics (COK) through the coordination of left and right limbs, which is highly related to joint mobility, muscle control, and limb coordination. The trajectory of the COK can fully reflect the overall characteristics of human walking. In contrast, the trajectory of the center of GRF (COF) is directly related to the smoothness and transformation speed in the GRF transition process between the left and right limbs.

Fig. 3 shows the proposed quantitative evaluation method of human walking balance ability based on COF and COK trajectory, which comprehensively considers human movement ability and limb coordination ability. Considering that falls often occur in the GRF transition process between the left and right limb [42], [43], [44], [45], this research focuses on the two key gait event frames of heel strike and toe off the ground, to evaluate the positional relationship between COF and COK, which is used to quantify the fall risk and assess the ability of walking balance.

Taking the right foot as an example, when the heel of the right foot is about to touch the ground, the GRF is all

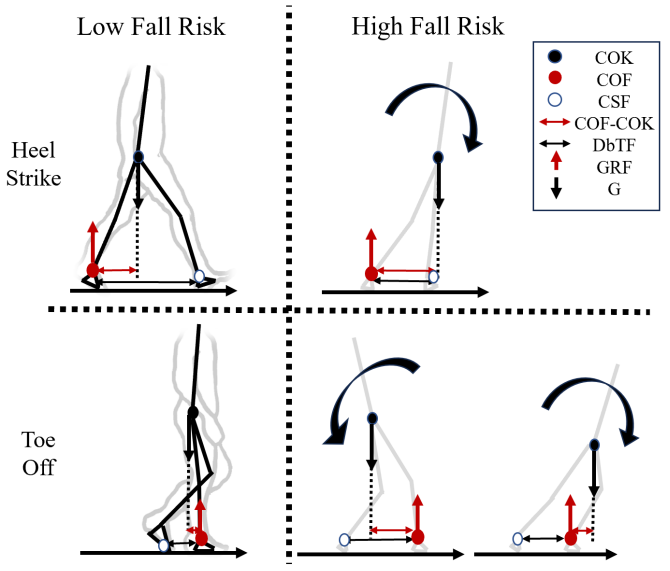

Fig. 3. Schematic diagram of walking balance ability assessment, where COK denotes the center of kinematics, COF denotes center of GRF, G denotes human gravity CSF denotes contralateral support foot, DbTF denotes distance between two feet.

distributed on the left foot. Meanwhile, the COM of the human body has moved to a position in front of the left foot. In low-fall-risk situations, the human COM is on the left side of the line connecting the left and right foot of the human body. At this moment, the torque of the human body's gravity on the right foot can effectively offset part of the torque of the left foot GRF on the right foot, so the left and right foot GRF can transition smoothly. In high-fall-risk situations, the COM is close to the right side of the line connecting the left and right foot. At this moment, the upper body is tilted forward, and the torque of the body's gravity on the right foot is significantly reduced or even reversed, which leads to the risk of falling forward.

Similarly, when analyzing the moment when the toe of the left foot is about to leave the ground, the center of rotation of the left foot is used for analysis. When the risk is low, the gravity of the human body can generate a large clockwise torque to the center of rotation, effectively offsetting the counterclockwise torque generated by the GRF, allowing the human body to walk normally. However, in the case of a high risk of falling, the counteracting torque produced by the body's gravity is greatly reduced. Therefore, the human body has a greater risk of falling backward at this time.

In another situation at this moment, The COK of the human body exceeds the COF. At this moment, although the moment generated by the human body's gravity is opposite to the direction of the moment generated by GRF, the length of the moment arm of the human body's gravity is much larger than that of GRF, which leads to a forward falling risk. Meanwhile, because the other foot has just left the ground, it is difficult to move to the front of the COK and support the human body quickly, leading to a high risk of falling. Eqs.(13) calculates the falling risk factor during walking.

$$\alpha(t) = \frac{x_{COK}(t) - x_{COF}(t)}{|x_{RA}(t) - x_{LA}(t)|} \tag{13}$$

where $\alpha(t)$ is the dynamic fall risk factor (DFRF) for subsequent walking balance quantification, x_{COK} and x_{COF} are the real-time trajectories of the motion center and GRF, respectively. The positive or negative difference between the two can directly reflect whether there is a forward or backward fall risk, x_{RA} and x_{LA} are the real-time trajectories of the left and right ankle joints, respectively.

Through above description, the real-time walking balance of the human body is established. However, the overall walking balance is needed. By studying changes in DFRF throughout the gait cycle, overall walking balance can be quantified. To this end, we divided the variation range of DFRF into three intervals: high fall risk interval A, medium fall risk interval B, and low-fall-risk interval C. As mentioned before, the greater the DFRF, the greater the fall may be at this time (because the GRF requirement that the foot can provide is more significant), so we set the high fall risk interval to be greater than 0.8; similarly, the medium risk interval and low-risk interval are The risk intervals are also defined as 0.5 and 0.3 respectively. After that, the proportion of DFRF in the three intervals within a complete gait cycle is weighted and summed. Considering the effects of high, medium, and low on human balance assessment, the three weights are 1, 0.5, and 0.1, respectively. The larger the sum value, the greater the time the subject spends in the high fall risk range during the entire walking process., The overall walking balance ability is weak. Eq. (12) calculates the overall fall risk index in the current cycle as:

$$CRI = \begin{bmatrix} \beta_1 & \beta_2 & \beta_3 \end{bmatrix} \begin{bmatrix} length(find(\alpha \in A)) \\ length(find(\alpha \in B)) \\ length(find(\alpha \in C)) \end{bmatrix} \tag{14}$$

where CRI is the comprehensive fall risk index, which is used to quantify the walking balance ability of human walking, $\begin{bmatrix} \beta_1 & \beta_2 & \beta_3 \end{bmatrix}$ are the amplification factors for high fall risk, medium fall risk, and low fall risk, respectively, and their values are $\begin{bmatrix} 1 & 0.5 & 0.1 \end{bmatrix}$, A, B, and C are the fall risk assessment intervals respectively, where $A = [0.8, \infty) \cup (-\infty, -0.8]$, $B = [0.5, 0.8) \cup (-0.8, -0.5]$, $C = [0.3, 0.5) \cup (-0.5, -0.3]$.

III. Results

A. Force-Sensing Shoe Accuracy Verification

Fig. 4 shows the accuracy verification results of the force-sensing shoes used to collect GRF in the gait experiment. To this end, we asked 6 healthy subjects to walk along the line three times, respectively, completing 18 gait experiments and aligning the starting points of the two groups of GRFs through the force generation points (when the measured GRF was greater than 5N). Due to the difference in sampling frequency of the two measurement systems (the sampling frequency of the force plate is 1000 Hz, and that of the force sensing shoe is 400 Hz), the isometric scaling method is used to reduce the sampling frequency of the two sets of GRFs to 200 Hz, so that the time axes of the two sets of GRFs are completely aligned. Finally, the normalized data of all subjects were averaged, and the standard deviation was calculated for subsequent verification of the accuracy of the sensing shoes.

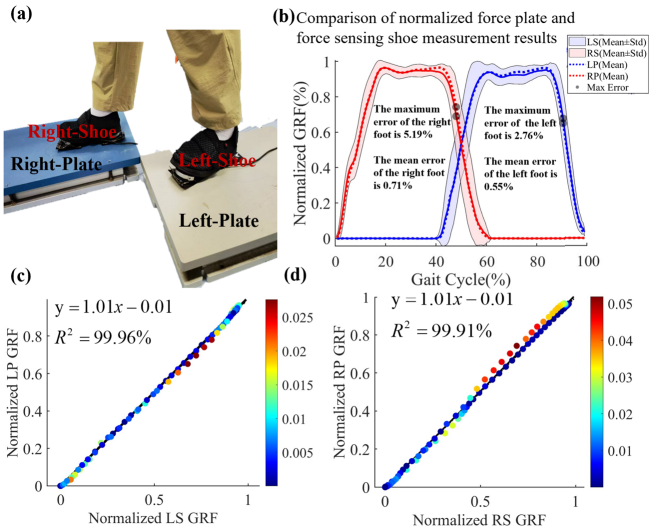

Fig. 4. Accuracy verification results of force-measuring shoes, where LS and RS represent the left and right shoes, respectively, LP and RP represent the left and right force plates, respectively. (a) Comparison between force shoes and force plates. (b) Comparison of two system in a complete gait cycle. (c) R-value distribution plot between two measurement systems of left foot. (d) R-value distribution plot between two measurement systems of right foot.

Fig. 4-(b) shows the time changes of the two types of GRF, which shows that their trends tend to be consistent. However, due to the different dynamic response capabilities of the two (different sampling frequencies), the GRF measurement time is slightly different between the two during high-speed changes (double support period), resulting in a small phase difference, which leads to more significant errors. And the second peak tracking effect of the sensing shoes is also slightly worse than the first peak. We speculate that the adaptability of the sensing shoes to different people's feet is not as good as that of regular sports shoes (because two rigid sensors are placed on the soles of the shoes). So, there will be a certain degree of slippage when the forefoot bears force, resulting in the second peak change not being fully tracked. This work uses the normalized mean absolute error (NMAE) and maximum error (NME) between two types of GRFs to better quantify the accuracy of the sensing shoe. The NMAE of the left and right feet are 0.55% and 0.71% respectively, while the NME are 2.76% and 5.19% respectively.

To show the accuracy of force-sensing shoes more intuitively, Fig. 4-(c) and Fig. 4-(d) compares the force-sensing shoe data (as the abscissa) and the force-measuring plate data (as the ordinate) in a complete cycle. Overall, the linearity of the curves is relatively good, and the R^2 of the left and right foot are 99.96% and 99.91%, respectively, indicating that the accuracy of the force-sensing shoes is trustworthy. Furthermore, it can be seen that the linearity of the force-sensing shoes is relatively good near the zero value and the maximum value. Still, the excessive force stage, there are a few points with large errors, especially the GRF of the right foot.

B. GRF Estimation

A single experiment generally consists of 10 to 20 gait cycle data (for an experiment with the same length of 10 meters, the number of gait cycles for health is less). Due to the

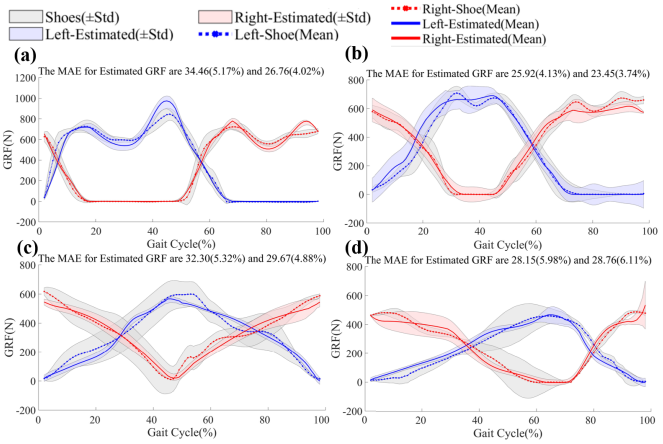

Fig. 5. Force estimation results of healthy subject 1, stroke patients 2, 10, and Parkinson's patients 8 for (a), (b), (c), and (d), respectively, where MAE denotes mean absolute error, Mean denotes the mean value of the error, Std denotes standard deviation of the error.

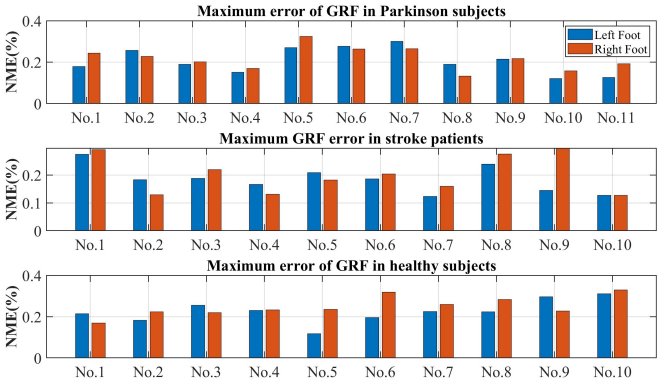

Fig. 6. Maximum GRF error in all subjects, where NME denotes normalized maximum absolute error.

lack of motion control, patients often have occasional and extremely abnormal gait data, significantly increasing the data interpretation difficulty. In this regard, we used Matlab's DBSCAN clustering method to filter the subjects' gait data to remove the accidental performance of the patient subjects and improve the data quality. Taking healthy subject 1, stroke patients 2, 10, and Parkinson's patients 8 as examples, Fig. 5 shows the estimated GRF results. All data are expressed as mean ± standard deviation (Mean ± std), which is used to visually compare the differences in gait stability between healthy subjects and patients. All the blue lines represent the GRF changes on the left foot, and the red lines represent the GRF changes on the right foot. The solid line represents the estimated GRF, and the dotted line represents the GRF directly measured by force shoes. Since the sampling frequency of IMUs is 100Hz, and the sampling frequency of force shoes is 400Hz, the data is scaled to 100Hz for synchronization. Similarly, the period of a gait cycle from the last left heel strike to the current left heel strike is scaled from 0 to 1 to show the variation of GRF more clearly.

As shown in Fig. 5-(a), the change of GRF of healthy subjects in a gait cycle is consistent with our knowledge and has a typical double peak curve. The duration of the single support period of the subject is longer than that of the double support period, and the GRF transition is smooth and fast in the double support period, indicating that the healthy subject has strong limb support and high stability. In addition, the peak value of the left and right foot, the time of the single support, period and the transition of the double support period are similar, indicating that the left and right limbs are symmetrical and do not show any unilateral hemiplegia, which also meet the definition of healthy subject.

For stroke patients, Fig. 5-(b) and Fig. 5-(c) show that the GRF estimated by the proposed model has a high consistency with the GRF directly measured by force shoes. Since subject 10 in Fig. 5-(c) has a much more severe stroke condition, the variation curves of GRF are highly inconsistent. Subject 2 in Fig. 5-(b) is in the late stage of rehabilitation, so the strength of the limbs has been fully recovered. Therefore, the transition time of GRF in the double support period is shorter and more stable than that of Subject 10. However, the hemiplegia gait caused by stroke still exists, which can be observed by the fact that the single support period time of the left foot (healthy side) is higher than that of the right foot (affected side), indicating that the muscle ability and balance ability of the left foot is much higher than those of the right foot. Subject 10, with a more severe condition, has a much longer double support period than the single support period. Furthermore, since the limb strength of both feet is very weak, the single-support period is so short that there is no typical double-peak curve. Fig. 5-(d) shows the GRF of Parkinson's patients, which is also significantly different from that of healthy subjects. It has no double peak curve, and the length of the double support period is much longer than that of the single support period.

The estimated GRF errors of 11 Parkinson's patients, 10 stroke patients, and 10 healthy subjects are collected in TABLE IV, where MAE and NMAE are used to quantify the estimation accuracy. At the same time, to more intuitively show the universality of the GRF estimation model to the three types of subjects, the average value of NMAE is also calculated. Considering that the average error can only reflect the overall performance of the GRF estimation algorithm and cannot fully reflect the algorithm's robustness, we also show the normalized maximum error (NME) of all subjects in Fig. 6. It can be seen that the maximum errors between healthy subjects and patients are evenly distributed around 20%, and there is no apparent difference in accuracy between the two.

C. Walking Balance Assessment

COF trajectories can be obtained based on the estimated GRF for all subjects. Combined with COK trajectories calculated based on the simplified human walking model, DFRF and CRI are calculated and shown in Fig. 7. The blue bars represent the DFRF when the left heel is on the ground (labeled LHS in the figure), the red bars are the DFRF when the right foot is off the ground (labeled RTO in the figure), the yellow bars are the DFRF when the right heel is on the ground (labeled RHS in the figure). The purple bars are the DFRF when the left foot is off the ground (labeled LTO in the figure).

TABLE IV
RESULTS OF ESTIMATED GRF

Subject	Parkinson's Patients		Stroke Patients		Healthy Subjects	
MAE(NMAE)	Left Foot	Right Foot	Left Foot	Right Foot	Left Foot	Right Foot
No.1	70.12(8.73%)	64.43(8.02%)	43.31(8.84%)	41.66(8.50%)	34.46(5.17%)	25.81(3.87%)
No.2	28.79(5.34%)	30.40(5.64%)	25.92(4.13%)	23.45(3.74%)	32.96(5.17%)	28.40(4.46%)
No.3	24.57(3.98%)	37.50(6.07%)	29.66(6.31%)	27.01(5.74%)	31.24(5.90%)	27.84(5.26%)
No.4	31.33(3.90%)	36.18(4.50%)	28.42(6.44%)	18.16(4.12%)	39.16(6.44%)	34.35(5.65%)
No.5	53.32(8.50%)	23.27(3.71%)	25.57(5.93%)	23.47(5.44%)	35.30(5.15%)	34.69(5.06%)
No.6	64.77(9.72%)	47.67(7.15%)	41.24(6.19%)	42.73(6.41%)	30.52(5.37%)	39.31(6.92%)
No.7	54.51(8.56%)	57.22(8.98%)	26.02(3.40%)	41.57(5.44%)	45.82(7.79%)	43.57(7.41%)
No.8	28.15(5.98%)	28.76(6.11%)	37.12(6.64%)	35.60(6.37%)	32.46(6.02%)	43.06(7.99%)
No.9	37.62(6.40%)	26.62(4.53%)	21.62(4.80%)	39.43(8.75%)	42.15(5.31%)	34.92(4.40%)
No.10	28.43(4.83%)	17.50(2.98%)	32.30(5.32%)	29.67(4.88%)	62.63(8.52%)	52.90(7.12%)
No.11	14.93(4.01%)	23.72(6.37%)	N.A	N.A	N.A	N.A
Mean NMAE	6.36%±2.17%	5.82%±1.82%	5.80%±1.51%	5.94%±1.66%	6.08%±1.19%	5.81%±1.44%

*MAE denotes mean absolute error, NMAE denotes the normalized mean absolute error.

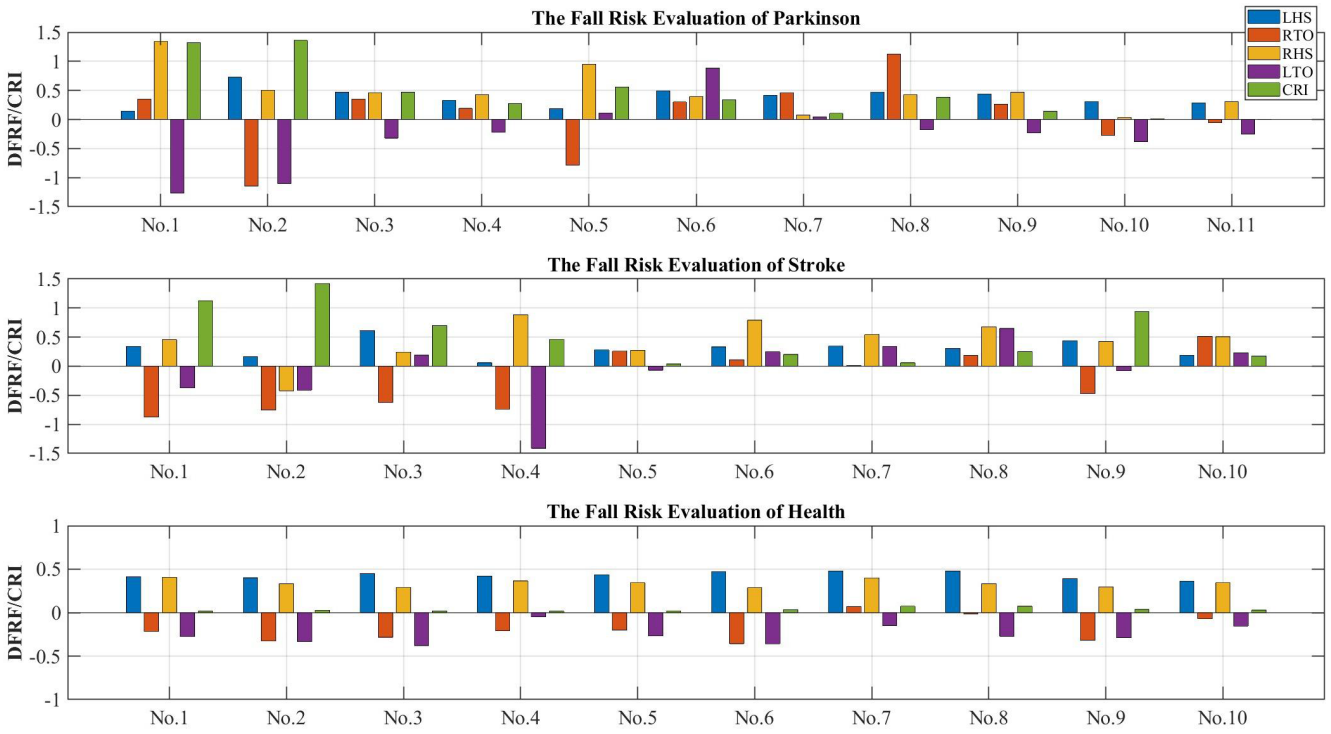

Fig. 7. DFRF and CRI of all subjects, where LHS denotes the DFRF when the left heel is on the ground, RTO denotes the DFRF when the right foot is off the ground, RHS denotes the DFRF when the right heel is on the ground, LTO denotes the DFRF when the left foot is off the ground.

And the green bars are the calculated CRI. The unit of CRI is second, which is different from DFRF. We draw 31 subjects in three subfigures according to the type of subjects.

It can be seen from the figure that the absolute value of DFRF of all healthy subjects is less than 0.5 at the selected four key gait event frames, which shows that healthy subjects have a good walking balance control ability regardless of their walking habits and walking speed. In contrast, the DFRF of Parkinson's disease subjects and stroke subjects is generally greater than 0.5 at four key gait event frames. Neurological diseases harm the body's balance control ability and increase the risk of falls. However, for some Parkinson's patients and stroke patients, such as Parkinson's subjects 10 and 11, their walking balance assessment results are close to those of healthy subjects, possibly due to these patient's limb functions have been fully restored. In addition, it was found that some patients, such as stroke subject 9, had low DFRF values at the selected four key gait event frames, but their CRI values were high. This indicates that although such patients were low fall risk at the heel-strike and toe-off moments, they had a high risk of falling at other times during walking. For the last category of patients, such as Parkinson's subject 7 and stroke subject 5,

their DFRF values and CRI values at the four moments are all at low levels, but the DFRF values at the toe-off moment are all positive. The position of COK is in front of COF, and there is a risk of falling forward. This is especially true for patients with slow movement. They have difficulty moving the limbs just off the ground quickly enough in front of COK to provide support. Therefore, the risk of falling for these patients is still high.

IV. Discussion

In this study, 11 Parkinson's patients, 10 stroke patients, and 10 healthy subjects were recruited to verify the proposed GRF estimation method and walking balance ability evaluation system. Compared with related works [23], [24], [25], [26], [27], [31], [32], one advantage of this research is that the number and types of subjects involved in this experiment are relatively large and diverse. The results also show that the method proposed in this paper is not only suitable for healthy subjects or patients with a single type of neurological disease but also has good adaptability to other types of walking patterns (such as hemiplegic gait of stroke patients or panic gait of Parkinson's patients), which fully verifies the clinical applicability of the model and method. In terms of the number of devices used, most of the current researches [24], [25] that can achieve GRF high precision (relative error less than 7%) uses a large number of IMUs (more than 5), which increases the difficulty of using the system and the motion interference to the user. This paper proposes a simplified walking model of four-link based on human anatomy data and human walking rules with only two IMUS placed on the shanks. The proposed system can fully capture motion data to reflect the overall human motion, and the proposed system can enhance the value of clinical applications.

In terms of GRF estimation, most of the current methods are verified on healthy subjects. The reason is that healthy subjects walk regularly and have a longer single support period. In this case, regression models or Newton-Euler equations are sufficient for high accuracy. However, for patients whose double support period is too long, these methods need help fully reflecting the change of GRF in the whole gait cycle. Moreover, the estimation of GRF based on IMUs is of more excellent in clinical practice because it is difficult for patients to bear the rigid structure and heavy weight of force-measuring shoes. The elastic elements and Newton-Euler equation hybrid driving GRF estimation method proposed in this paper uses the deformation process of the virtual elastic elements of the shank and thigh within the double support period to map the GRF change process and uses the Newton-Euler equation to directly calculate the single support GRF changes, to realize the GRF estimation for patients with neurological diseases.

Besides, this paper proposes a balance assessment method based on the relative position between COK and COF and successfully compares the differences between healthy subjects, Parkinson's patients, and stroke patients. Different from existing balance assessment researches, this paper develops the balance ability assessment work through a simple hardware system and further quantifies whether the risk of falling forward or backward will occur at key time points during walking, which provides new ways for fall prediction in clinical rehabilitation scenarios or home-based elderly life scenarios.

However, this paper also has the following limitations. First of all, although the current sample size of this paper is better than that of similar works (as shown in TABLE I), it is still needs to be added to the actual clinical application. Whether the proposed method can be fully adapted to different types of patients remains to be further verified. Second, this paper's walking balance assessment method is only used to compare the differences between Parkinson's patients, stroke patients, and healthy subjects. The walking balance assessment method is more in line with clinical needs in assessing the recovery of a specific patient during the rehabilitation process, which needs further collection and analysis of patient data. The third is that the healthy subjects recruited in this paper are generally younger than the patients as control samples, which will inevitably introduce external factors into evaluating walking balance ability.

V. Conclusion

This paper proposes a GRF indirect estimation method, which captures motion data that can reflect the overall walking characteristics of the human body through a simplified four-link model and two IMUs placed on shanks. Based on the elastic elements and Newton-Euler equation hybrid driving method, the proposed method can conduct the GRF estimation of the human's full gait cycle. The GRF estimation method is verified on recruited 10 healthy subjects, 11 Parkinson's patients, and 10 stroke patients, and the NMAE is controlled at about 6%. In addition, based on the estimated GRF and the acquired motion data, this paper also proposes a walking balance ability assessment method based on the positional relationship between COF and COK. It evaluates the overall balance performance and fall risk at four critical moments during walking. The method proposed in this paper has a simple hardware system, which is convenient and can be used in real-time. It can be used for clinical rehabilitation process evaluation and fall risk assessment for the older people at home.

References

[1] Y. Moon, J. Sung, R. An, M. E. Hernandez, and J. J. Sosnoff, "Gait variability in people with neurological disorders: A systematic review and meta-analysis," *Human Movement Sci.*, vol. 47, pp. 197–208, Jun. 2016.

[2] R. Barclay-Goddard, T. Stevenson, W. Poluha, M. E. K. Moffatt, and S. P. Taback, "Force platform feedback for standing balance training after stroke," *Stroke*, vol. 36, no. 2, pp. 412–413, Feb. 2005.

[3] A. Mansfield and E. L. Inness, "Force plate assessment of quiet standing balance control: Perspectives on clinical application within stroke rehabilitation," *Rehabil. Process Outcome*, vol. 4, Jan. 2015, Art. no. S20363.

[4] P. Jogi, A. Zecevic, T. J. Overend, S. J. Spaulding, and J. F. Kramer, "Force-plate analyses of balance following a balance exercise program during acute post-operative phase in individuals with total hip and knee arthroplasty: A randomized clinical trial," *SAGE Open Med.*, vol. 4, Jan. 2016, Art. no. 205031211667509.

[5] R. E. Mayagoitia, J. C. Lötters, P. H. Veltink, and H. Hermens, "Standing balance evaluation using a triaxial accelerometer," *Gait Posture*, vol. 16, no. 1, pp. 55–59, Aug. 2002.

[6] F. Parisi et al., "Inertial BSN-based characterization and automatic UPDRS evaluation of the gait task of parkinsonians," *IEEE Trans. Affect. Comput.*, vol. 7, no. 3, pp. 258–271, Jul. 2016.

[7] L. Wang, Y. Sun, Q. Li, T. Liu, and J. Yi, "IMU-based gait normalcy index calculation for clinical evaluation of impaired gait," *IEEE J. Biomed. Health Informat.*, vol. 25, no. 1, pp. 3–12, Jan. 2021.

[8] P. Ismailidis et al., "Measuring gait kinematics in patients with severe hip osteoarthritis using wearable sensors," *Gait Posture*, vol. 81, pp. 49–55, Sep. 2020.

[9] J. Xu et al., "Configurable, wearable sensing and vibrotactile feedback system for real-time postural balance and gait training: Proof-of-concept," *J. Neuroeng. Rehabil.*, vol. 14, no. 1, pp. 1–10, Dec. 2017.

[10] R. Mc Ardle et al., "Gait in mild Alzheimer's disease: Feasibility of multi-center measurement in the clinic and home with body-worn sensors: A pilot study," *J. Alzheimer's Disease*, vol. 63, no. 1, pp. 331–341, 2018.

[11] J. Howcroft, J. Kofman, E. D. Lemaire, and W. E. McIlroy, "Analysis of dual-task elderly gait in fallers and non-fallers using wearable sensors," *J. Biomech.*, vol. 49, no. 7, pp. 992–1001, May 2016.

[12] H. Zhou et al., "Assessment of gait and balance impairment in people with spinocerebellar ataxia using wearable sensors," *Neurol. Sci.*, vol. 43, no. 4, pp. 2589–2599, Apr. 2022.

[13] R. P. Hubble, G. A. Naughton, P. A. Silburn, and M. H. Cole, "Wearable sensor use for assessing standing balance and walking stability in people with Parkinson's disease: A systematic review," *PLoS ONE*, vol. 10, no. 4, Apr. 2015, Art. no. e0123705.

[14] S. Díaz, J. B. Stephenson, and M. A. Labrador, "Use of wearable sensor technology in gait, balance, and range of motion analysis," *Appl. Sci.*, vol. 10, no. 1, p. 234, Dec. 2019.

[15] S. A. Alves, R. M. Ehrig, P. C. Raffalt, A. Bender, G. N. Duda, and A. N. Agres, "Quantifying asymmetry in gait: The weighted universal symmetry index to evaluate 3D ground reaction forces," *Frontiers Bioeng. Biotechnol.*, vol. 8, Oct. 2020, Art. no. 579511.

[16] J. Fagert et al., "Structure- and sampling-adaptive gait balance symmetry estimation using footstep-induced structural floor vibrations," *J. Eng. Mech.*, vol. 147, no. 2, Feb. 2021, Art. no. 04020151.

[17] M. M. Rieger, S. Papegaaij, F. Steenbrink, M. Pijnappels, and J. H. van Dieën, "Development of a balance recovery performance measure for gait perturbation training based on the center of pressure," *Frontiers Sports Act. Living*, vol. 3, Feb. 2021, Art. no. 617430.

[18] E. Martini et al., "Pressure-sensitive insoles for real-time gait-related applications," *Sensors*, vol. 20, no. 5, p. 1448, Mar. 2020.

[19] M. V. McCabe, D. W. Van Citters, and R. M. Chapman, "Developing a method for quantifying hip joint angles and moments during walking using neural networks and wearables," *Comput. Methods Biomech. Biomed. Eng.*, vol. 26, no. 1, pp. 1–11, Jan. 2023.

[20] A. I. Kubba and A. A. Ameen, "Gait cycle ground reaction force measurement using piezoelectric sensor attached to shoe-insole system," *IOP Conf., Mater. Sci. Eng.*, vol. 881, no. 1, Jul. 2020, Art. no. 012063.

[21] F. Salis, S. Bertuletti, T. Bonci, U. D. Croce, C. Mazzà, and A. Cereatti, "A method for gait events detection based on low spatial resolution pressure insoles data," *J. Biomech.*, vol. 127, Oct. 2021, Art. no. 110687.

[22] R. Eguchi, A. Yorozu, T. Fukumoto, and M. Takahashi, "Estimation of vertical ground reaction force using low-cost insole with force plate-free learning from single leg stance and walking," *IEEE J. Biomed. Health Informat.*, vol. 24, no. 5, pp. 1276–1283, May 2020.

[23] E. Shahabpoor, A. Pavic, J. M. W. Brownjohn, S. A. Billings, L.-Z. Guo, and M. Bocian, "Real-life measurement of tri-axial walking ground reaction forces using optimal network of wearable inertial measurement units," *IEEE Trans. Neural Syst. Rehabil. Eng.*, vol. 26, no. 6, pp. 1243–1253, Jun. 2018.

[24] A. Karatsidis et al., "Estimation of ground reaction forces and moments during gait using only inertial motion capture," *Sensors*, vol. 17, no. 1, p. 75, Dec. 2016.

[25] T. Tan, D. P. Chiasson, H. Hu, and P. B. Shull, "Influence of IMU position and orientation placement errors on ground reaction force estimation," *J. Biomechanics*, vol. 97, Dec. 2019, Art. no. 109416.

[26] M. I. M. Refai, B. F. van Beijnum, J. H. Buurke, and P. H. Veltink, "Portable gait lab: Estimating 3D GRF using a pelvis IMU in a foot IMU defined frame," *IEEE Trans. Neural Syst. Rehabil. Eng.*, vol. 28, no. 6, pp. 1308–1316, Jun. 2020.

[27] M. S. B. Hossain, Z. Guo, and H. Choi, "Estimation of lower extremity joint moments and 3D ground reaction forces using IMU sensors in multiple walking conditions: A deep learning approach," *IEEE J. Biomed. Health Informat.*, vol . 27, no. 6, pp. 2829–2840, Jun. 2023, doi: 10.1109/JBHI.2023.3262164.

[28] M. M. Bach, N. Dominici, and A. Daffertshofer, "Predicting vertical ground reaction forces from 3D accelerometry using reservoir computers leads to accurate gait event detection," *Frontiers Sports Act. Living*, vol. 4, Oct. 2022, Art. no. 1037438.

[29] J. Camargo, A. Ramanathan, W. Flanagan, and A. Young, "A comprehensive, open-source dataset of lower limb biomechanics in multiple conditions of stairs, ramps, and level-ground ambulation and transitions," *J. Biomech.*, vol. 119, Apr. 2021, Art. no. 110320.

[30] T. Tan, D. Wang, P. B. Shull, and E. Halilaj, "IMU and smartphone camera fusion for knee adduction and knee flexion moment estimation during walking," *IEEE Trans. Ind. Informat.*, vol. 19, no. 2, pp. 1445–1455, Feb. 2023.

[31] Z. Ripic, C. Kuenze, M. S. Andersen, I. Theodorakos, J. Signorile, and M. Eltoukhy, "Ground reaction force and joint moment estimation during gait using an Azure Kinect-driven musculoskeletal modeling approach," *Gait Posture*, vol. 95, pp. 49–55, Jun. 2022.

[32] M. Eltoukhy, C. Kuenze, M. S. Andersen, J. Oh, and J. Signorile, "Prediction of ground reaction forces for Parkinson's disease patients using a Kinect-driven musculoskeletal gait analysis model," *Med. Eng. Phys.*, vol. 50, pp. 75–82, Dec. 2017.

[33] T. Li, F. Chen, Z. Zhao, Q. Pei, Y. Tan, and Z. Zhou, "Hybrid data-driven optimization design of a layered six-dimensional FBG force/moment sensor with gravity self-compensation for orthopedic surgery robot," *IEEE Trans. Ind. Electron.*, vol. 70, no. 8, pp. 8568–8579, Aug. 2023.

[34] A. F. Azocar, L. M. Mooney, L. J. Hargrove, and E. J. Rouse, "Design and characterization of an open-source robotic leg prosthesis," in *Proc. 7th IEEE Int. Conf. Biomed. Robot. Biomechatronics*, Aug. 2018, pp. 111–118.

[35] L. Gabert and T. Lenzi, "Instrumented pyramid adapter for amputee gait analysis and powered prosthesis control," *IEEE Sensors J.*, vol. 19, no. 18, pp. 8272–8282, Sep. 2019.

[36] P. de Leva, "Adjustments to Zatsiorsky–Seluyanov's segment inertia parameters," *J. Biomech.*, vol. 29, no. 9, pp. 1223–1230, Sep. 1996.

[37] X. Liu, B. Zhou, B. Zhang, and T. Liu, "A potential-real-time thigh orientation prediction method based on two shanks-mounted IMUs and its clinical application," *IEEE Trans. Autom. Sci. Eng.*, doi: 10.1109/TASE.2022.3232632.

[38] R. Fluit, M. S. Andersen, S. Kolk, N. Verdonschot, and H. F. J. M. Koopman, "Prediction of ground reaction forces and moments during various activities of daily living," *J. Biomech.*, vol. 47, no. 10, pp. 2321–2329, Jul. 2014.

[39] Y. Jung, M. Jung, J. Ryu, S. Yoon, S.-K. Park, and S. Koo, "Dynamically adjustable foot-ground contact model to estimate ground reaction force during walking and running," *Gait Posture*, vol. 45, pp. 62–68, Mar. 2016.

[40] E. Shahabpoor and A. Pavic, "Estimation of vertical walking ground reaction force in real-life environments using single IMU sensor," *J. Biomech.*, vol. 79, pp. 181–190, Oct. 2018.

[41] M. A. Sherman, A. Seth, and S. L. Delp, "Simbody: Multibody dynamics for biomedical research," *Procedia IUTAM*, vol. 2, pp. 241–261, Jan. 2011.

[42] A. F. Polcyn, L. A. Lipsitz, D. C. Kerrigan, and J. J. Collins, "Age-related changes in the initiation of gait: Degradation of central mechanisms for momentum generation," *Arch. Phys. Med. Rehabil.*, vol. 79, no. 12, pp. 1582–1589, Dec. 1998.

[43] D. A. Schieb, "Walkway surface heights and ground reaction forces," in *Proc. 14th Southern Biomed. Eng. Conf.*, Apr. 1995, pp. 175–178.

[44] A. J. Clark and T. E. Higham, "Slipping, sliding and stability: Locomotor strategies for overcoming low-friction surfaces," *J. Exp. Biol.*, vol. 214, no. 8, pp. 1369–1378, Apr. 2011.

[45] J. Gragg and J. Yang, "Potential methods for prediction of onset of slip in gait during the transition from double support to single support," in *Proc. Int. Design Eng. Tech. Conf., Comput. Inf. Eng. Conf.*, vol. 55898. New York, NY, USA: American Society of Mechanical Engineers, 2013, Paper no. V03BT03A021.